Annals of Biomedical Engineering, Vol. 36, No. 7, July 2008 *(© 2008)* pp. 1152–1162
DOI: 10.1007/s10439-008-9502-3

Characterization of Coherent Structures in the Cardiovascular System

SHAWN C. SHADDEN and CHARLES A. TAYLOR

Department of Bioengineering, Stanford University, Stanford, CA, USA

(Received 9 January 2008; accepted 10 April 2008; published online 25 April 2008)

Abstract—Recent advances in blood flow modeling have provided highly resolved, four-dimensional data of fluid mechanics in large vessels. The motivation for such modeling is often to better understand how flow conditions relate to health and disease, or to evaluate interventions that affect, or are affected by, blood flow mechanics. Vessel geometry and the pulsatile pumping of blood leads to complex flow, which is often difficult to characterize. This article discusses a computational method to better characterize blood flow kinematics. In particular, we compute Lagrangian coherent structures (LCS) to study flow in large vessels. We demonstrate that LCS can be used to characterize flow stagnation, flow separation, partitioning of fluid to downstream vasculature, and mechanisms governing stirring and mixing in vascular models. This perspective allows valuable understanding of flow features in large vessels beyond methods traditionally considered.

Keywords—Hemodynamics, Computational fluid dynamics, Biofluid mechanics, Finite-time Lyapunov exponents, Lagrangian coherent structures.

INTRODUCTION

Knowledge of blood flow mechanics is critical to understanding the hemodynamic factors that lead to acute and gradual changes in the function and health of vessels. For example, regions of disrupted flow have been correlated to the localization of atherosclerosis,[19,42] recirculation in the infrarenal abdominal aorta is hypothesized to contribute to the development of abdominal aortic aneurysms (AAAs),[3,33] and quantification of flow distribution and characteristics is becoming important in evaluating the benefits of surgical intervention.[17,30,31,40,41] However, quantifying important flow features has been a challenge.

Current *in vivo* (e.g., phase-contrast magnetic resonance imaging (PC-MRI)[15]), *in vitro* (e.g., particle image velocimetry (PIV)[1]) and computational methods[41] for quantifying blood flow typically produce Eulerian velocity data as output. The velocity field itself has limited clinical relevance. It measures the instantaneous rate of change of particle positions. One is typically more interested in the transport of the fluid or forces produced by the fluid motion. Although it is often reasonable to infer the qualitative, or bulk, fluid motion from inspection of the velocity data, mentally piecing together the time history of velocity fields to quantify flow structures can easily result in misinterpretations when the velocities are time-dependent. Likewise, measures computed from the instantaneous velocity data, e.g. streamlines, vorticity, Q-criterion, rate-of-strain, etc., are similarly unreliable for understanding unsteady fluid behavior. Nonetheless, inherently Lagrangian characteristics, such as flow recirculation, stagnation, and separation, are often quantified in cardiovascular applications using these instantaneous Eulerian measures.

Tracking the fluid motion directly (Lagrangian perspective) can be achieved by computing particle trajectories from integrating the velocity data or adding tracers (e.g., "dye") in the flow during *in vivo* or *in vitro* experiments. Quantifying the fluid motion is often difficult because, even in highly laminar flow, particle trajectories can be chaotic,[20] and stirring/mixing can make relevant flow features, if any, difficult to distinguish. There is a tradeoff. Instantaneous Eulerian measures are convenient for visualization, but often do not result in an accurate understanding of the true fluid motion, whereas visualizing the fluid motion directly gives the complete, nonlinear fluid behavior, but makes quantification difficult and *ad hoc*.

The purpose of this article is to demonstrate a method to better understand fundamental transport structures and mechanisms in complex, 3D cardiovascular flows. The computation of Finite-Time Lyapunov Exponent (FTLE) fields provides a scalar measure that accounts for the unsteady, nonlinear behavior of the fluid, but can be visualized as an Eulerian field. Furthermore, FTLE fields reveal flow features, known as Lagrangian coherent structures

Address correspondence to Shawn C. Shadden, Department of Bioengineering, Stanford University, Stanford, CA, USA. Electronic mail: sshadden@gmail.com, taylorca@stanford.edu

0090-6964/08/0700-1152/0 © 2008 Biomedical Engineering Society

(LCS), that yield insight into how fluid is transported. We demonstrate that this perspective can be used to quantify the extent of flow stagnation, determine where and how flow separates, understand how flow is partitioned to downstream vasculature, and reveal the mechanisms governing stirring and mixing in large vessels.

METHODS

Blood Flow Modeling

In vivo and *in vitro* measurements of blood flow tend to be under-resolved for identifying the complete flow structure in large vessels. To understand the hemodynamic features present in a particular region of interest, one must typically rely on computational blood flow modeling to achieve a satisfactory level of resolution. To demonstrate the computation of LCS, blood flow in models of a carotid bifurcation; a generic and a patient-specific AAA; and a total cavopulmonary connection (TCPC) are studied. The models shown herein were constructed from custom software for image-based modeling.[40] The model of the carotid bifurcation and the generic AAA are idealized models, with dimensions derived from patient-specific data. The overall geometries of the carotid bifurcation and generic AAA are representative of models previously studied in the literature to allow for comparison. The patient-specific AAA and TCPC models were constructed from magnetic resonance (MR) angiography data.

Each geometric model was discretized using a commercial tetrahedral mesh generator (www.simmetrix.com) to produce a computational mesh. Blood flow was simulated by solving the Navier–Stokes equations over the mesh using a stabilized finite-element method.[9,32,38]

For all simulations, a Newtonian approximation for the fluid viscosity was assumed ($\mu = 0.04$ g cm^{-1} s^{-1}), the fluid density was assumed constant ($\rho = 1.06$ g cm^{-3}), and a rigid wall approximation was employed. For inlet boundary conditions, the time-varying volumetric flow entering each model was mapped to a time-varying parabolic profile over the inlet of the model. This was done for two inlets in the TCPC model. For outlet boundary conditions, the coupled multidomain method was employed.[35] Depending on the application, either resistance, impedance, or RCR (Windkessel model) was used at model outlets to represent the downstream vasculature, with parameters tuned to produce physiologic pressure and flow distributions. The results of these computations were used to demonstrate the computation of LCS.

LCS

Definitions

Solving the Navier–Stokes equations provides the velocity field $\mathbf{v}(\mathbf{x}, t)$. The position of a fluid particle as a function of time, $\mathbf{x}(t)$, is assumed to be governed by

$$\dot{\mathbf{x}}(t) = \mathbf{v}(\mathbf{x}, t). \tag{1}$$

Integration of Eq. (1) from time t to $t + \tau$ provides the flow map $\phi_t^{t+\tau} : \mathbf{x}(t) \mapsto \mathbf{x}(t+\tau)$. The FTLE is defined as

$$\sigma(\mathbf{x}, t, \tau) = \frac{1}{2|\tau|} \ln \lambda_{\max}(\mathbf{S}(\mathbf{x}, t, \tau)), \tag{2}$$

where

$$\mathbf{S}(\mathbf{x}, t, \tau) = \left(\frac{d\phi_t^{t+\tau}(\mathbf{x}(t))}{d\mathbf{x}(t)}\right)^{\mathrm{T}} \left(\frac{d\phi_t^{t+\tau}(\mathbf{x}(t))}{d\mathbf{x}(t)}\right) \tag{3}$$

is a finite-time version of the right Cauchy–Green deformation tensor and $\lambda_{\max}(\mathbf{S}(\mathbf{x}, t, \tau))$ denotes the maximum eigenvalue of $\mathbf{S}(\mathbf{x}, t, \tau)$, where $\mathbf{S}(\mathbf{x}, t, \tau)$ is thought of as a linear operator.

The FTLE can be considered a measure of how sensitive a trajectory is to perturbations. For example, if we let $\boldsymbol{\delta}(t)$ be a perturbation to $\mathbf{x}(t)$ at time t, then it can be shown[28] that

$$\|\boldsymbol{\delta}(t+\tau)\| \leq e^{\sigma(\mathbf{x},t,\tau)|\tau|} \|\boldsymbol{\delta}(t)\|. \tag{4}$$

That is, a perturbation will have at most an exponential growth rate factor of $\sigma(\mathbf{x}, t, \tau)$. Equality holds in Eq. (4) when $\boldsymbol{\delta}(t)$ is aligned with the eigenvector associated with $\lambda_{\max}(\mathbf{S}(\mathbf{x}, t, \tau))$. However, the growth of almost all perturbations approximately satisfy Eq. (4) since the dynamics are quickly dominated by the projection of the perturbation in this eigenvector direction, a property that has sometimes been used to simplify the computation of the FTLE.

The spatial distribution of the FTLE field can be used to detect dominant features in the flow.[7,22] In particular, LCS are defined as co-dimension one structures that locally maximize the FTLE field transverse to the structure.[14,28] For 2D flows, LCS correspond to curves of high FTLE, and for 3D flows, LCS correspond to surfaces of high FTLE.

It is well-known that for unsteady systems, the fluid motion can be chaotic, even when the velocity field is very predictable and laminar. The sensitivity of fluid trajectories is often due to turning points in the flow. These turning points are sometimes referred to as hyperbolic trajectories.[8,39] While they qualify as trajectories, and hence can have complex motion themselves, they do not always qualify as hyperbolic. Nonetheless, their stability properties and influence on surrounding fluid is robust. LCS allow us to

understand how the influence of these turning points extends throughout the domain. This is key to understanding transport in a range of fluid flow problems.

It is advantageous to look at the sensitivity of particle paths to initial placement both in forward time and when time is reversed ($\tau < 0$). LCS obtained from the *forward time* FTLE field (where particles are mapped to their location at some later time) are referred to as *repelling* LCS and LCS obtained from the *backward time* FTLE are referred to as *attracting* LCS. As the name implies, attracting LCS are surfaces to which fluid is attracted. In this sense, attracting LCS often correspond to flow features revealed by injecting a contrast agent into a fluid, however the attracting LCS provide a more precise outline of these material surfaces (as contrast agents can diffuse, obscuring these surfaces).

Computation Method

To compute the spatial variation of the FTLE field, i.e. $\sigma(\mathbf{x}, t, \tau)$ for t and τ fixed, a mesh of particles is seeded in the domain of interest at time t. The trajectory of each particle is obtained by numerically integrating Eq. (1) from t to $t + \tau$. For the present analyses, a Runge–Kutta–Fehlberg integration scheme[5] was used with a maximum error tolerance of 10^{-6} and a maximum time step size set so that particles move less than the smallest edge size in the velocity data mesh each integration time step. Velocity data was computed on a high resolution tetrahedral mesh and linear basis functions were used to interpolate the data during the integration of particle paths.

The final position of each particle provides the flow map. The deformation tensor, Eq. (3), can then be computed by finite differencing data from neighboring mesh points. The maximum eigenvalue of the deformation tensor and subsequently the FTLE are then computed. The FTLE value for each particle in the mesh is assigned to the particle location at time t, not $t + \tau$. This process is then repeated varying the evaluation time t to get the time variation of the FTLE field.

The considerations in choosing an appropriate integration time τ are the extent of the LCS sought, the amount of available data, and computational expense. The first is a theoretical concern and the latter two are computational concerns.

In general, one should choose an integration time commensurate with the time-scale of the dynamics of interest. For example, if one is interested in quantifying transport over one cardiac cycle, then an integration length of one cardiac is reasonable for computing the FTLE field. As the integration time increases, the integrated effect of various time scales are captured. Therefore large integration times may produce LCS corresponding to flow features from different time scales. This is not necessarily undesirable, but can make interpretation difficult if the FTLE field becomes convoluted with LCS. Fortunately, numerous computations have shown that the location of LCS is relatively unaffected by changes in the integration time. Therefore, the choice of integration time is typically not critical from a theoretical perspective.

In practice, however, the integration time is usually dictated by computational concerns. Often the deciding factor is the amount of available velocity data, both in space and time. For the examples studied here, the velocity field can be assumed to repeat each cardiac cycle, thus there is no temporal limitation. However, once a particle is advected out of the spatial domain of the velocity data, integration must cease and the FTLE is computed for that point based on an integration time set to when the particle left the domain if it is less than the desired integration time. Eventually, most particles become flushed from the domain, and choosing an integration time beyond this will not change the FTLE field.

Visual inspection of the FTLE field is often sufficient to interpret the location and behavior of the LCS. In some instances, systematically extracting the LCS is desired. This is often of interest when trying to separate a given LCS from other ones present, or when an exact parametrization is needed for further analysis. For such cases we use an extraction method based on the definition of LCS.[25]

LCS are defined as lines (in 2D) or surfaces (in 3D) that locally maximize the FTLE field. That is, transverse to the LCS the FTLE is at a local maximum and therefore the gradient of the FTLE field, $\nabla\sigma(\mathbf{x}, t, \tau)$ is aligned with the LCS and the eigenvector $\mathbf{v}_{\min}(\mathbf{x}, t, \tau)$ corresponding to the minimum eigenvalue of the Hessian of the FTLE field $\lambda_{\min}(d^2\sigma/d\mathbf{x}^2)$ is transverse to the LCS (for precise definitions, see Lekien *et al.*[14] and Shadden *et al.*[28]). Therefore the scalar field

$$\alpha(\mathbf{x}, t, \tau) = \langle \nabla\sigma(\mathbf{x}, t, \tau),\ \mathbf{v}_{\min}(\mathbf{x}, t, \tau) \rangle \qquad (5)$$

is constant (equal to zero) along LCS. Zero level sets of α define LCS when two conditions are satisfied: the minimum eigenvalue of the Hessian of the FLTE field is negative, and $\mathbf{S}(\mathbf{x}, t, \tau)$ has one and only one eigenvalue greater than one. Therefore, LCS can be extracted by plotting zero level sets of α where these two conditions are satisfied. We can threshold these level sets based on the values of $\sigma(\mathbf{x}, t, \tau)$ or $\lambda_{\min}(d^2\sigma/d\mathbf{x}^2)$ to extract the most well-defined structures. This method usually performs well if the FTLE grid spacing is small enough so that neighboring LCS provide distinct maxima.

RESULTS

Carotid Bifurcation

A 3D computational model of a human carotid bifurcation was constructed to replicate the model of Bharadvaj *et al.*[2] This geometry was based on measurements obtained from 57 angiograms from 22 normal patients between 34 and 77 years old.

At the inlet of the common carotid artery (CCA), we prescribed a pulsatile, periodic flow waveform taken from Marshall *et al.*[18] scaled to have a period of 0.923 s. At the outlets of the internal and external carotid arteries (ICA and ECA), impedance boundary conditions were used to ensure a proper flow distribution between the ICA and ECA,[18] and a physiologic pressure pulse of 120/70 mmHg.[13]

Solutions to the Navier–Stokes equations were obtained from a 382,961 element and 73,723 node nonuniform, tetrahedral mesh with a time step size of 0.000923 s. The solution was computed for five cardiac cycles to ensure solution convergence. Velocity data was output every 0.01846 s over the last cardiac cycle for post-processing.

The velocity data was used to computed the backward time FTLE field over the cardiac cycle. Inspection of the backward time FTLE field shows an attracting LCS that extends from the proximal end of the carotid sinus, Fig. 1. The LCS is shown at four times during the cardiac cycle—early systole, peak systole, early diastole, and mid diastole. The LCS is well-defined over almost the entire cardiac cycle.

Idealized AAA

An idealized model of a AAA was constructed to study flow patterns in a fusiform aneurysm, with a geometry similar to models previously studied.[4,21,24,34] The dimensions for the model are given in Fig. 2. The curvature of the aneurysm is elliptic. The diameter of the aorta, maximal diameter of the aneurysm, length of the aneurysm, and diameter of the common iliac arteries are representative of measurements taken from patient-specific image data; this image data was used to construct the patient-specific model considered in the section "Patient-specific AAA."

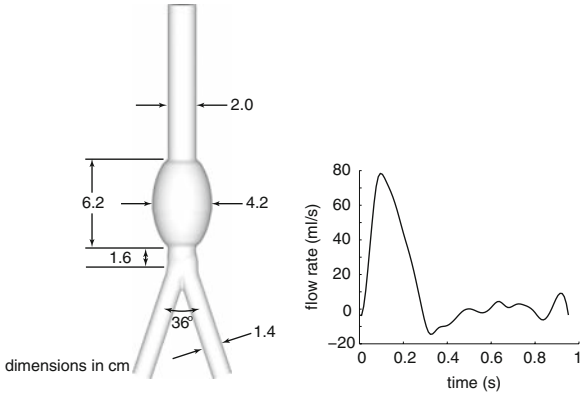

FIGURE 2. Idealized AAA geometry and inflow waveform. The period of the cardiac cycle is 0.952 s.

A patient-specific infrarenal waveform measured from PC-MRI was used as the inflow boundary condition, Fig. 2. Resistance boundary conditions were specified at the outlets of the iliac arteries, with equal resistance at each outlet, and total resistance set to produce a physiologic pressure pulse.

The computational mesh used for solving Navier–Stokes equations consisted of a 614,100 element and 117,315 node tetrahedral mesh. The simulation time-step size was 0.000952 s and the solution was computed over five cardiac cycles to ensure convergence. Over the last cardiac cycle, velocity data was output every 0.00238 s for post-processing.

The velocity data was used to compute the forward and backward time FTLE fields over the cardiac cycle. The backward time FTLE fields reveal an attracting LCS as shown in Fig. 3 and the forward time FTLE fields reveal a repelling LCS as shown in Fig. 4. These plots show an upper level set of the FTLE field, which

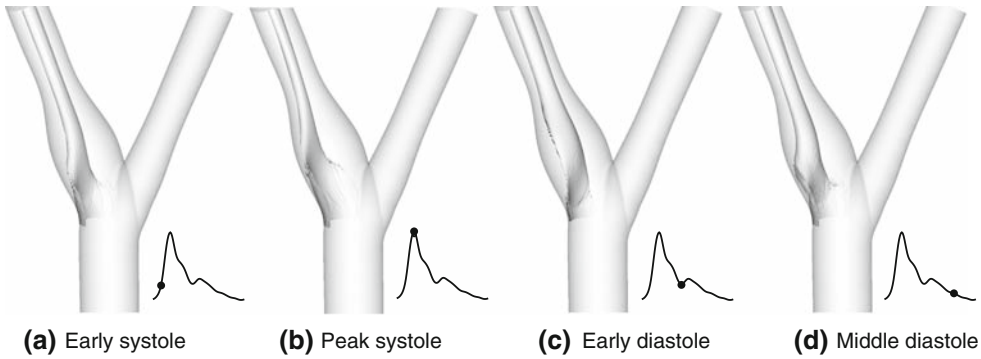

FIGURE 1. Evolution of attracting LCS in the carotid sinus over the cardiac cycle. This LCS captures the unsteady separation profile in the carotid sinus providing a clear, geometric representation of the separation.

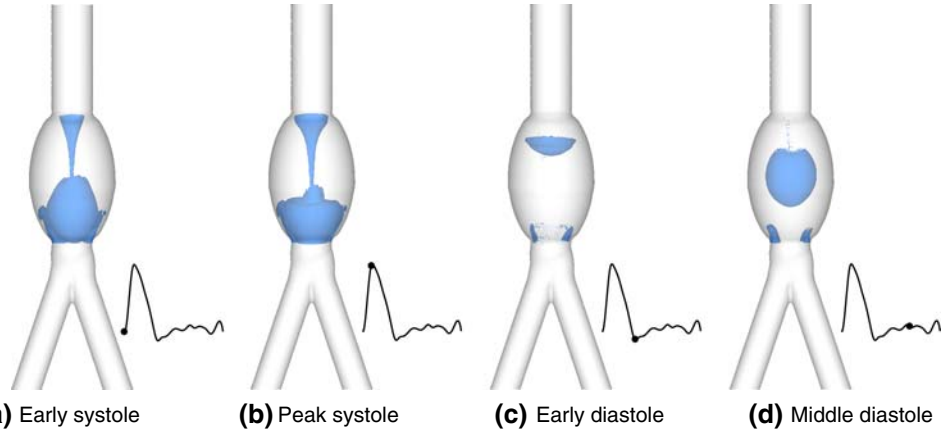

FIGURE 3. Evolution of attracting LCS inside idealized AAA over the cardiac cycle.

can often be used to approximate the location of the LCS.[28]

Although 3D rendering techniques continue to improve, it is often necessary to restrict visualization to 2D sections to better understand the geometrical structure. Due to the symmetry of the model, coronal sections of the forward and backward time FTLE fields inside the aneurysm during mid-diastole are shown in Fig. 5. This figure also shows the residence time field, which measures the time it takes fluid to be flushed from the aneurysm. The regions shaded dark blue correspond to fluid that remains in the aneurysm longer than one cardiac cycle.

Patient-specific AAA

MR angiography was performed on a 78-year-old male with a moderate-sized AAA. The MR data was used to construct a geometric model that spanned from the supraceliac aorta to below the iliac bifurcation, including the celiac, superior mesenteric and renal arteries, as shown in Fig. 6. The volumetric flow through the supraceliac and infrarenal aorta was measured *in vivo* from PC-MRI under resting conditions. The supraceliac flow rate (cf. Fig. 6) was used to specify the inlet boundary condition and combined with the infrarenal flow rate to help tune outlet boundary conditions. The computational model consisted of an adapted,[23] tetrahedral mesh of 71,1270 elements and 135,289 nodes. Impedance boundary conditions were specified at the outlets. The simulation time step used to solve Navier–Stokes equations was set to 0.000968 s.

The Reynolds number at peak systole reaches approximately 1150 in the infrarenal aorta (proximal to the aneurysm) and is less than 500 mid-aneurysm, based on the mean velocity (volumetric flow rate divided by the cross-sectional area of the vessel) and the effective diameter of the vessel. Fully developed turbulence was not observed, however inspection of the velocity data does reveal transient (weak) turbulence inside the aneurysm. This is in contrast with the idealized AAA model that, although having similar Reynolds numbers, produced flow that is completely laminar. Since the Navier–Stokes equations are solved directly (without a turbulence model), a relatively

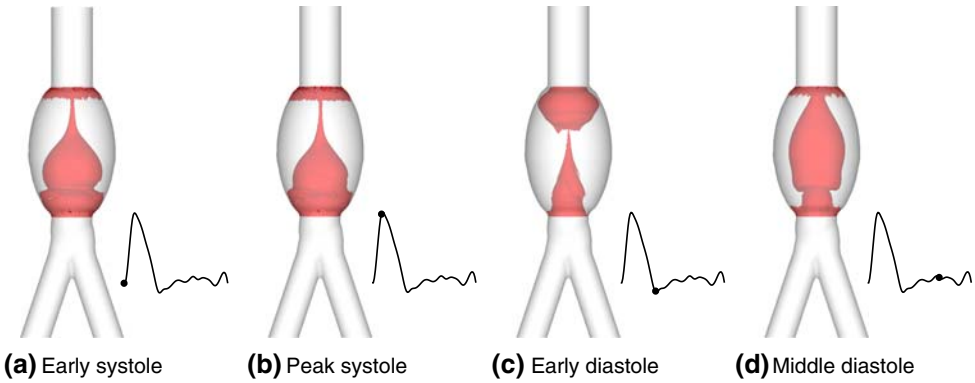

FIGURE 4. Evolution of repelling LCS inside idealized AAA over the cardiac cycle.

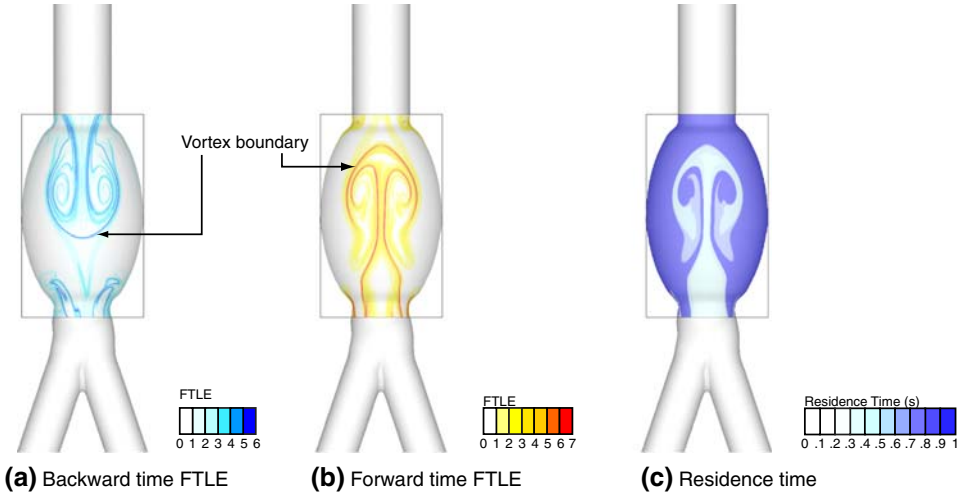

FIGURE 5. Cross-sectional view of FTLE and residence time fields during mid-diastole.

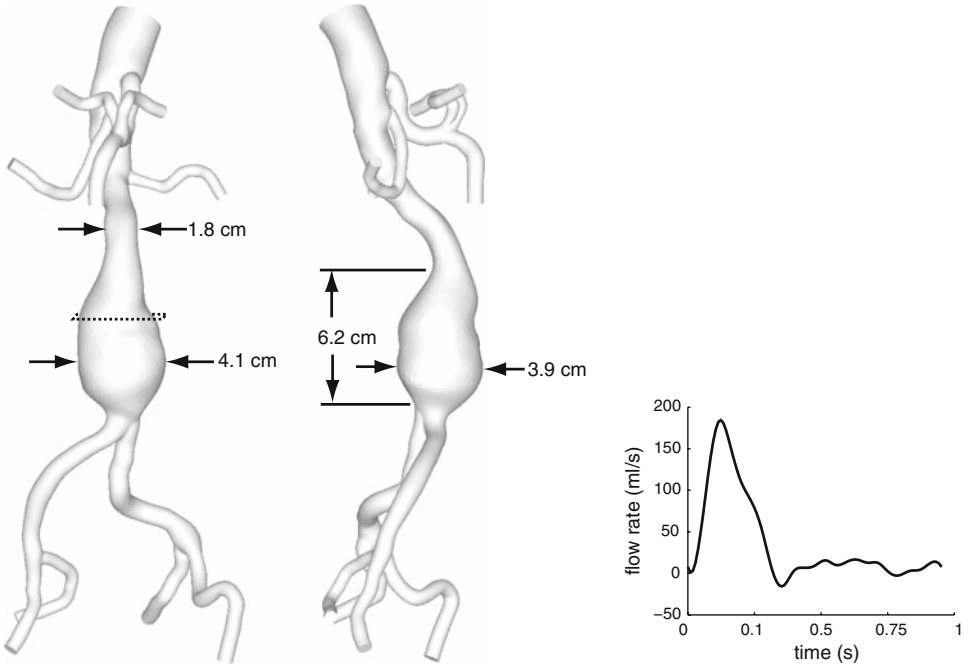

FIGURE 6. Patient-specific AAA model and input supraceliac flow rate.

high-resolution finite-element mesh is needed to resolve the length scales in the velocity field. Although the mesh used in this analysis is under-resolved, additional, higher-resolution computations have been performed that confirm similar unsteadiness in the aneurysm as the data analyzed here.

The forward time FTLE field was computed in the aneurysm. The field has a much more complex distribution than in the idealized model. However, LCS can still be observed. For such complex flow, plotting the full 3D LCS is difficult to visualize. Instead, a cross-section of the FTLE field shown in the left panel of Fig. 7, taken spatially at an arbitrary location in the aneurysm near the proximal end, and temporally near the end of systole.

To demonstrate the correlation between the LCS and regions of stagnation, the residence time of the fluid at this cross-section was computed and is shown in the right panel of Fig. 7. Areas colored orange correspond to blood that remains in the aneurysm longer than one cardiac cycle. To compare the repelling LCS with the residence time field, we algorithmically extract the LCS from the FTLE field, as described in the section "Computation method." The left panel

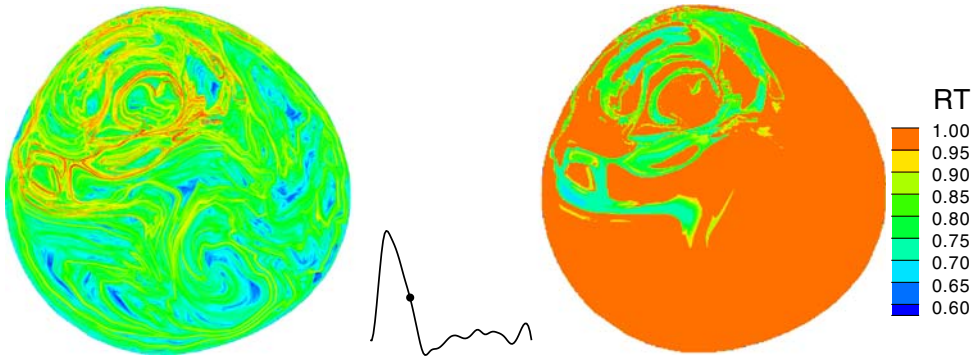

FIGURE 7. (Left) Cross-section of 3D FTLE field in the aneurysm. Cross-section taken at location of dotted-lines in Fig. 6. The integration time used to compute the FTLE was equal to one cardiac cycle. (Right) Residence time at planar section where FTLE is shown. Color map is specified in seconds.

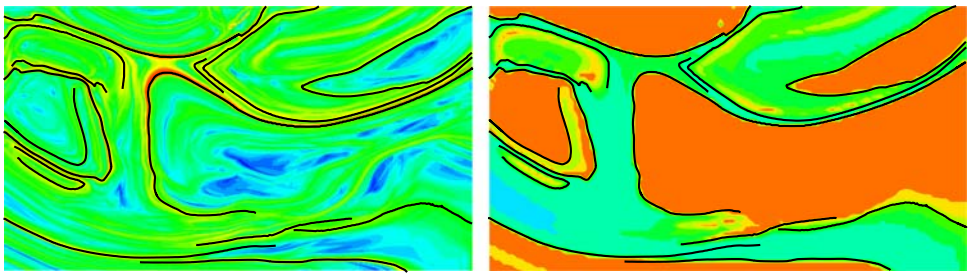

FIGURE 8. (Left) Close up of FTLE field showing extracted LCS. (Right) Close up of residence time plot with extracted LCS. The LCS correspond closely to the boundaries between stagnant flow and flow that is quickly flushed from the AAA.

of Fig. 8 shows a close-up of the result of this extraction procedure and the right panel of Fig. 8 superimposes these extracted LCS with the residence time field.

TCPC

Recently, a modification to the configuration of the total cavopulmonary connection (Fontan procedure) was proposed.[16] This modification incorporates a Y-graft connection of the inferior vena cava (IVC) to the pulmonary arteries. A patient-specific computational model of the TCPC was constructed from MR angiography data taken from imaging a 4-year-old male with a traditional TCPC. Once the patient-specific model was constructed, a new geometric model was created by replacing the IVC connection with a Y-graft connection, while retaining the rest of the patient-specific geometry unaltered, resulting in the model shown in Fig. 9.

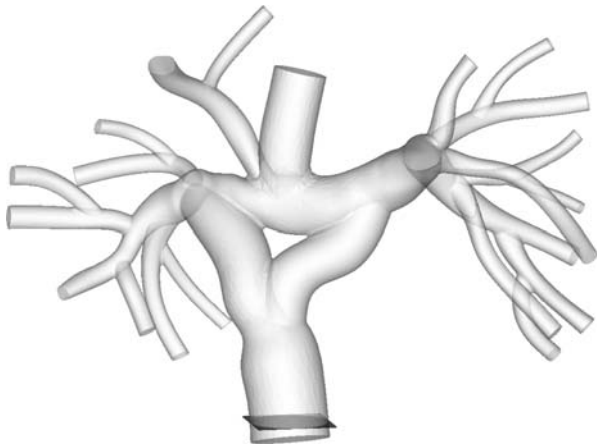

FIGURE 9. Model of total cavopulmonary connection. Plots shown in Fig. 10 correspond to location of shaded plane shown near the inlet of the IVC.

The nonuniform, tetrahedral mesh used to solve the Navier–Stokes equations over the model consisted of 1,154,685 elements and 224,448 nodes. The simulation step size was 0.0005 s. For boundary conditions, the volumetric flow rates through the IVC and superior vena cava (SVC) were measured from PC-MRI and were used to prescribe inflow boundary conditions at the IVC and SVC inlets.[17] At the 20 outlets of the pulmonary arteries, a 3-element windkessel model[37] was assigned using the coupled multidomain method.[35] The resistances and capacitance of each windkessel model were chosen to fit the impedance of a morphometry-based arterial tree at each outlet.[29]

A motivation for the Y-graft connection is to provide better distribution of IVC flow to the pulmonary arteries to help prevent pulmonary arteriovenous

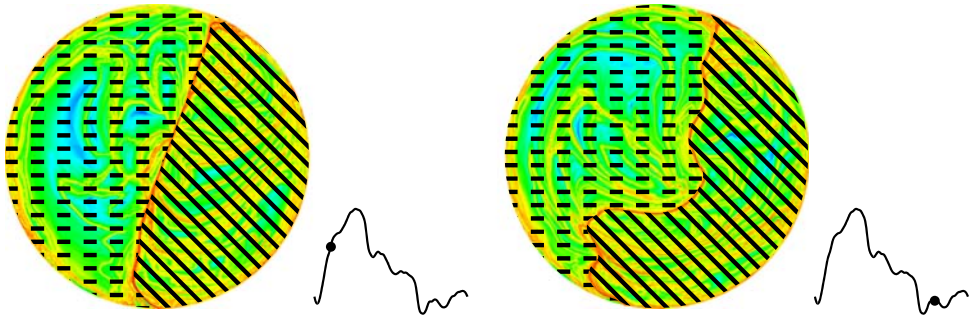

FIGURE 10. Cross-section of the FTLE field near the inlet of the IVC reveals an LCS that partition the IVC flow between the right pulmonary arteries (dashed region) and left pulmonary arteries (slanted lines) at two points in the respiratory cycle. Note, in this simulation IVC flow is periodic with the respiratory, not cardiac, cycle.

malformations due to unequal distribution of hepatic venous flow.[10] To better understand how IVC flow is distributed, the forward time FTLE field was computed near the inlet of the IVC. Figure 10 shows a cross-section of the FTLE field during inspiration (left) and expiration (right) near the IVC inlet. The FTLE fields reveal several LCS, including a well-defined LCS that partitions fluid transported through the right or left branches of the Y-graft.

DISCUSSION

Carotid Bifurcation

Previous studies have noted the correlation between flow separation in the carotid bifurcation and atherosclerotic plaque deposition. Difficulty in visualizing unsteady separation and in obtaining quantitative flow information in the carotid bifurcation were noted.[11,12] This led to a simplified representation of the fluid mechanics by focusing on the distribution of wall shear stress (WSS). Correlations between low WSS and high oscillatory shear index (OSI)[12] to atherosclerosis were noted, yet these measures provide limited insight into the hemodynamic mechanisms responsible for these correlations.

Separation occurs when fluid flowing along a wall pulls away from the wall due to an adverse pressure gradient. Locally, the flow converges to a separation profile.[36] If time is reversed, opposite behavior is observed, with fluid approaching the wall along the separation profile and then diverging. Computing the backward time FTLE helps reveal this surface of separation. The attracting LCS shown in the carotid model represents the profile along which flow separates in the carotid sinus. We see that the edges of the separation surface roll up into neighboring spirals, which extend down the ICA. Separation occurs over nearly the entire cardiac cycle, although the profile varies over time. Being able to visualize the separation allows a better understanding into *why* certain regions may have low WSS or high OSI and a better understanding of how fluid is transported.

Differences in patient anatomy result in varying susceptibility to flow separation, therefore it is often difficult to predict whether a particular anatomy gives way to adverse hemodynamics. The framework presented here enables a clear understanding of when separation is present and the ability to characterize the separation profile. Detecting separation is important due to the correlation with disease localization and loss of hemodynamic efficiency.

Idealized AAA

Previous studies have noted the formation of vortices in fusiform aneurysms.[4,21,24] However quantification of flow recirculation and stagnation is often missing. Since recirculation and stagnation presumably play an important role in thrombus formation and inflammatory mechanisms, it is important to be able to quantify these conditions. For the fusiform aneurysm studied in the section "Idealized AAA," during systole blood travels down the infrarenal aorta and separates from the aorta at the proximal end of the aneurysm, resulting in the shedding of a laminar vortex ring during early diastole.

Shadden *et al.*[26,27] demonstrated that LCS can be used to capture the boundary of vortex rings generated from a piston-cylinder apparatus and that the LCS predict which fluid is entrained (detrained) to (from) the vortex. Similarly, superimposing the attracting and repelling LCS in this AAA model gives the boundary of the vortices formed in each cardiac cycle. The LCS that provide these boundaries are noted in Fig. 5.

The non-dimensional vortex formation time,[6] $\bar{U}\Delta t/D$, is approximately 2.0, where $\bar{U} = 14.7\,\mathrm{cm\,s^{-1}}$ is the average infrarenal flow rate during systole, $\Delta t = 0.27$ s the duration of systole, and $D = 2.0$ cm the infrarenal aortic diameter (proximal to the aneurysm).

Formation times of laminar vortex rings less than 4–5 typically result in all circulation being transferred to a single vortex.[6] Therefore we might expect that the main mechanism transporting blood through the aneurysm is the propagation of the vortex rings. The LCS enable delineation of the exact boundary of the vortex and thus quantification of the vortex volume, which was computed to be 11.0 cm^3. Integrating the suprarenal volumetric flow rate over systole gives 12.3 cm^3. So indeed, nearly all fluid traveling down the infrarenal aorta is imparted to the vortex.

Comparing the location of the repelling LCS shown in Fig. 5b with the residence time field shown in Fig. 5c demonstrates that fluid bound by the LCS is primarily the fluid that is flushed from the aneurysm in less than one cardiac cycle, whereas fluid outside the LCS remains confined to this region over that period of time. Therefore, the repelling LCS is a *separatrix* that, in addition to capturing the vortex boundary, delineates the boundary of stagnant regions.

Patient-Specific AAA

The patient-specific AAA model produces more complex flow than the idealized AAA model. Although the Reynolds number in the infrarenal aorta is similar, the complexity of the vessel geometry induces turbulent behavior in the aneurysm. Characterizing turbulent flow has long been a challenge for many problems, and being able to identify detailed flow structures in 3D turbulence is exceptionally difficult. While the flow in the aneurysm is not homogeneous turbulence, it is clear from inspection of the velocity data that rapid fluctuations of the velocity in space and time are present and the flow no longer has a laminar structure. While the efficacy of computing LCS in 3D turbulent or near-turbulent flow has not been fully explored, the results of section "Patient-specific AAA" are encouraging.

The complex distribution of FTLE suggest complex stirring of fluid in the aneurysm. Nonetheless, the FTLE distribution provides well-defined LCS. Similar to the idealized AAA model, Fig. 8 shows that there is a strong correlation between the location of the repelling LCS and the boundaries of stagnant flow in the aneurysm. However, particles can be seeded on either side of the LCS, as done for the idealized AAA model, to better understand why these regions have high residence time. We can also notice that even in regions of stagnation, that there are LCS appearing which indicates that substantial stirring and mixing is occurring in this region, even though the fluid remains in the aneurysm over the cardiac cycle.

The existence of LCS in 3D turbulence is very interesting, but in such applications visualization and parameterization of the LCS can become difficult, and thus further advances related to these issues are needed.

TCPC

For the TCPC, we examined the structure of the LCS near the inlet of the model in the IVC. The motivation for this was to characterize flow distributed between the left and right pulmonary branches. There is a well-defined LCS that partitions the flow between the left and right pulmonary branches; in Fig. 10 the region advected through the left conduit is filled with the slanted solid lines and the fluid advected through the right conduit is filled by the horizonal dashed lines. Tracking the location of that LCS enables quantification of how much IVC flow goes to the left or right pulmonary arteries; in this case 45% of IVC flow is distributed to the left conduit and 55% of IVC flows is distributed to the right conduit. This 45–55 flow split is in direct proportion to the ratio of peripheral resistances. That is, the bulk distribution of IVC flow is dictated by downstream boundary conditions. This is in contrast to the tradition "T-junction" and "offset" TCPC models,[16] which when analyzed showed preferential distribution of flow based on the local configuration of the connection.

Inspection of the FTLE fields also reveal several more LCS, which partition how the flow is distributed between more distal arterial branches. Although the LCS were used in this example to determine the bulk distribution of IVC flow between the LPA's and RPA's, the LCS provide a *spatial* understanding of how flow is distributed to the distal vasculature. For example, if one is interested in where an embolus is likely to travel in a particular model, an exhaustive number of simulations varying the initial position of the embolus in a particular vicinity could be run to determine where the embolus is likely to be transported. Alternatively, a more complete, geometric understanding can be obtained by computing LCS in the region the emboli are likely to form. Such knowledge could also be beneficial in drug targeting or surgical planning.

CONCLUSIONS

Flow in large vessels is unsteady. Often 3D, laminar, or weakly turbulent, flow structures are present, especially at locations of pathology. Previous studies of blood flow mechanics have typically employed traditional Eulerian criteria to visualize the hemodynamics. The unsteadiness of the velocity field makes these criteria unreliable. To better characterize the behavior

of the fluid, a Lagrangian perspective is often required. Although particle motion can be complex and difficult interpret directly, the FTLE condenses trajectory information to a scalar measure. The remarkable property of this measure is that it enables extraction of an underlying transport structure by revealing so-called LCS. These LCS help to identify key separatrices dictating transport and help generalize intuitive concepts, such as flow separation or vortex boundaries, that are otherwise difficult to define rigorously for unsteady flow.

To demonstrate this method, we applied the computation of LCS to regions of the vasculature where flow has been associated with pathological conditions. These examples enabled us to demonstrate the utility of this method to better characterize clinically relevant flow conditions, such as, flow stagnation, flow separation, partitioning of fluid to downstream vasculature, and mechanisms governing stirring and mixing. We believe this method may offer a breakthrough in studying flow behavior in the cardiovascular system, including aiding in understanding the role of fluid mechanics in disease progression, evaluating medical device or surgical design, and as a tool to better diagnose unfavorable hemodynamics.

ACKNOWLEDGMENTS

The authors would like to sincerely thank Alison Marsden and Adam Bernstein for the TCPC velocity data and Andrea Les for the patient-specific AAA velocity data. The authors gratefully acknowledge the use of the AcuSolve linear algebra package (http://www.acusim.com) and the MeshSim automatic mesh generator (http://www.simmetrix.com). S. Shadden was supported by an NSF Mathematical Sciences Postdoctoral Research Fellowship. This work was also supported by the National Institutes of Health (P50 HL083800, U54 GM072970) and the National Science Foundation under Grant No. 0205741.

REFERENCES

[1]Adrian, R. J. Particle imaging techniques for experimental fluid mechanics. *Annu. Rev. Fluid Mech.* 23:261–304, 1991.
[2]Bharadvaj, B. K., R. F. Mabon, and D. P. Giddens. Steady flow in a model of the human carotid bifurcation. Part I—Flow visualization. *J. Biomech.* 15(5):349–362, 1982.
[3]Bluestein, D., L. Niu, R. T. Schoephoerster, and M. K. Dewanjee. Steady flow in an aneurysm model: correlation between fluid dynamics and blood platelet deposition. *J. Biomech. Eng.* 118(3):280–294, 1996.
[4]Egelhoff, C. J., R. S. Budwig, D. F. Elger, T. A. Khraishi, and K. H. Johansen. Model studies of the flow in abdominal aortic aneurysms during resting and exercise conditions. *J. Biomech.* 32(12):1319–1329, 1999.
[5]Fehlberg, E. Low-order classical Runge-Kutta formulas with step size control and their application to some heat transfer problems. *NASA Technical Report*, 315, 1969.
[6]Gharib, M., E. Rambod, and K. Shariff. A universal time scale for vortex ring formation. *J. Fluid Mech.* 360:121–140, 1998.
[7]Haller, G. Distinguished material surfaces and coherent structures in three-dimensional fluid flows. *Physica D* 149(4):248–277, 2001.
[8]Haller, G., and A. C. Poje. Finite time transport in aperiodic flows. *Physica D* 119(3–4):352–380, 1998.
[9]Jansen, K. E., C. H. Whiting, and G. M. Hulbert. Generalized-alpha method for integrating the filtered Navier-Stokes equations with a stabilized finite element method. *Comput. Methods Appl. Mech. Eng.* 190(3):305–319, 2000.
[10]Justino, H., L. N. Benson, and R. M. Freedom. Development of unilateral pulmonary arteriovenous malformations due to unequal distribution of hepatic venous flow. *Circulation* 103(8):E39–E40, 2001.
[11]Ku, D. N., and D. P. Giddens. Pulsatile flow in a model carotid bifurcation. *Arteriosclerosis* 3(1):31–39, 1983.
[12]Ku, D. N., D. P. Giddens, C. K. Zarins, and S. Glagov. Pulsatile flow and atherosclerosis in the human carotid bifurcation: positive correlation between plaque location and low and oscillating shear-stress. *Arteriosclerosis* 5(3):293–302, 1985.
[13]Laurent, S., J. Cockcroft, L. Van Bortel, P. Boutouyrie, C. Giannattasio, D. Hayoz, B. Pannier, C. Vlachopoulos, I. Wilkinson, and H. Struijker-Boudier. Expert consensus document on arterial stiffness: methodological issues and clinical applications. *Eur. Heart J.* 27(21):2588–2605, 2006.
[14]Lekien, F., S. C. Shadden, and J. E. Marsden. Lagrangian coherent structures in *n*-dimensional systems. *J. Math. Phys.* 48(6):065404, 2007.
[15]Markl, M., F. P. Chan, M. T. Alley, K. L. Wedding, M. T. Draney, C. J. Elkins, D. W. Parker, R. Wicker, C. A. Taylor, R. J. Herfkens, and N. J. Pelc. Time-resolved three-dimensional phase-contrast MRI. *J. Magn. Reson. Imaging* 17(4):499–506, 2003.
[16]Marsden, A. L., A. Bernstein, V. M. Reddy, S. C. Shadden, R. L. Spilker, F. P. Chan, C. A. Taylor, and J. A. Feinstein. Evaluation of a novel Y-shaped extracardiac Fontan baffle using computational fluid dynamics. *J. Thorac. Cardiovasc. Surg.* (submitted).
[17]Marsden, A. L., I. E. Vignon-Clementel, F. Chan, J. A. Feinstein, and C. A. Taylor. Effects of exercise and respiration on hemodynamic efficiency in CFD simulations of the total cavopulmonary connection. *Ann. Biomed. Eng.* 35(2):250–263, 2007.
[18]Marshall, I., P. Papathanasopoulou, and K. Wartolowksa. Carotid flow rates and flow division at the bifurcation in healthy volunteers. *Physiol. Meas.* 25(3):961–967, 2004.
[19]Moore, J. E., C. Xu, S. Glagov, C. K. Zarins, and D. N. Ku. Fluid wall shear stress measurements in a model of the human abdominal aorta: oscillatory behavior and relationship to atherosclerosis. *Atherosclerosis* 110(2):225–240, 1994.
[20]Ottino, J. M. The Kinematics of Mixing: Stretching, Chaos, and Transport. New York: Cambridge University Press, 1989.
[21]Peattie, R. A., T. J. Riehle, and E. I. Bluth. Pulsatile flow in fusiform models of abdominal aortic aneurysms: flow

fields, velocity patterns and flow-induced wall stresses. *J. Biomech. Eng*. 126(4):438–446, 2004.
[22]Pierrehumbert, R. T. Large-scale horizontal mixing in planetary atmospheres. *Phys. Fluids A* 3(5):1250–1260, 1991.
[23]Sahni, O., J. Muller, K. E. Jansen, M. S. Shephard, and C. A. Taylor. Efficient anisotropic adaptive discretization of the cardiovascular system. *Comput. Methods Appl. Mech. Eng*. 195(41–43):5634–5655, 2006.
[24]Salsac, A. V., S. R. Sparks, and J. C. Lasheras. Hemodynamic changes occurring during the progressive enlargement of abdominal aortic aneurysms. *Ann. Vasc. Surg*. 18(1):14–21, 2004.
[25]Shadden, S. C. *A dynamical systems approach to unsteady systems*. PhD thesis, California Institute of Technology, 2006.
[26]Shadden, S. C., J. O. Dabiri, and J. E. Marsden. Lagrangian analysis of fluid transport in empirical vortex rings. *Phys. Fluids* 18(4):047105, 2006.
[27]Shadden, S. C., K. Katija, M. Rosenfeld, J. E. Marsden, and J. O. Dabiri. Transport and stirring induced by vortex formation. *J. Fluid Mech*. 593:315–331, 2007.
[28]Shadden, S. C., F. Lekien, and J. E. Marsden. Definition and properties of Lagrangian coherent structures from finite-time Lyapunov exponents in two-dimensional aperiodic flows. *Physica D* 212(3–4):271–304, 2005.
[29]Spilker, R. L., J. Feinstein, D. Parker, V. M. Reddy, and C. A. Taylor. Morphometry-based impedance boundary conditions for patient-specific modeling of blood flow in pulmonary arteries. *Ann. Biomed. Eng*. 35(4):546–559, 2007.
[30]Taylor, C. A., and M. T. Draney. Experimental and computational methods in cardiovascular fluid mechanics. *Annu. Rev. Fluid Mech*. 36:197–231, 2004.
[31]Taylor, C. A., M. T. Draney, J. P. Ku, D. Parker, B. N. Steele, K. Wang, and C. K. Zarins. Predictive medicine: computational techniques in therapeutic decision-making. *Comput. Aided Surg*. 4(5):231–247, 1999.
[32]Taylor, C. A., T. J. R. Hughes, and C. K. Zarins. Finite element modeling of blood flow in arteries. *Comput. Methods Appl. Mech. Eng*. 158(1–2):155–196, 1998.
[33]Taylor, C. A., T. J. R. Hughes, and C. K. Zarins. Finite element modeling of three-dimensional pulsatile flow in the abdominal aorta: relevance to atherosclerosis. *Ann. Biomed. Eng*. 26(6):975–987, 1998.
[34]Taylor, T. W., and T. Yamaguchi. Three-dimensional simulation of blood flow in an abdominal aortic aneurysm: Steady and unsteady flow cases. *J. Biomech. Eng*. 116(1):89–97, 1994.
[35]Vignon-Clementel, I. E., C. A. Figueroa, K. E. Jansen, and C. A. Taylor. Outflow boundary conditions for three-dimensional finite element modeling of blood flow and pressure in arteries flow and pressure in arteries. *Comput. Methods Appl. Mech. Eng*. 195(29–32):3776–3796, 2006.
[36]Wang, K. C. On the current controversy about unsteady separation. In: Numerical and Physical Aspects of Aerodynamic Flows, edited by T. Cebeci. Springer, 1982.
[37]Westerhof, N., F. Bosman, C. J. De Vries, and A. Noordergraaf. Analog studies of the human systemic arterial tree. *J. Biomech*. 2(2):121–143, 1969.
[38]Whiting, C. H., and K. E. Jansen. A stabilized finite element method for the incompressible Navier-Stokes equations using a hierarchical basis. *Int. J. Numer. Methods Fluids* 35(1):93–116, 2001.
[39]Wiggins, S. The dynamical systems approach to Langrangian transport in oceanic flows. *Annu. Rev. Fluid Mech*. 37:295–328, 2005.
[40]Wilson, N., F. R. Arko, and C. A. Taylor. Patient-specific operative planning for aorto-femoral reconstruction procedures. *Lect. Notes Comput. Sci*. 3217:422–429, 2004.
[41]Wilson, N., K. Wang, R. Dutton, and C. A. Taylor. A software framework for creating patient specific geometric models from medical imaging data for simulation based medical planning of vascular surgery. *Lect. Notes Comput. Sci*. 2208:449–456, 2001.
[42]Zarins, C. K., D. P. Giddens, B. K. Bharadvaj, V. S. Sottiurai, R. F. Mabon, and S. Glagov. Carotid bifurcation atherosclerosis: quantitative correlation of plaque localization with flow velocity profiles and wall shear stress. *Circ. Res*. 53(4):502–514, 1983.